JCI insight

Multiparametric immune profiling in HPV$^-$ oral squamous cell cancer

Zipei Feng, … , Barbara Seliger, Bernard A. Fox

JCI Insight. 2017;2(14):e93652. https://doi.org/10.1172/jci.insight.93652.

Research Article | Immunology | Oncology

Evaluation of T lymphocyte frequency provides prognostic information for patients with oral squamous cell cancer (OSCC). However, the effect of simultaneously evaluating T cell frequency and assessing suppressive elements and defects in antigen-processing machinery (APM) has not been clarified. Simultaneous characterization of CD3$^+$, CD8$^+$, FoxP3$^+$, CD163$^+$, and PD-L1$^+$ cells using multispectral imaging was performed on sections from 119 patients with HPV$^-$ OSCC. Expression of β_2-microglobulin, MHC class I heavy chain, and large multifunctional peptidase 10 was quantified, and all data were correlated with patient outcome. We found that, consistent with previous reports, high numbers of CD8$^+$ T cells at the invasive margin correlated significantly with prolonged overall survival (OS), while the number of FoxP3$^+$ or PD-L1$^+$ cells did not. Compiling the number of FoxP3$^+$ or PD-L1$^+$ cells within 30 μm of CD8$^+$ T cells identified a significant association with a high number of suppressive elements close to CD8$^+$ T cells and reduced OS. Integrating this information into a cumulative suppression index (CSI) increased correlation with OS. Incorporating tumor expression levels of APM components with CSI further improved prognostic power. This multiparametric immune profiling may be useful for stratifying patients with OSCC for clinical trials.

Find the latest version:

https://jci.me/93652/pdf



JCI insight

RESEARCH ARTICLE

Multiparametric immune profiling in HPV$^-$ oral squamous cell cancer

Zipei Feng,[1,2] Daniel Bethmann,[1,3] Matthias Kappler,[4] Carmen Ballesteros-Merino,[1] Alexander Eckert,[4] R. Bryan Bell,[1,5] Allen Cheng,[5] Tuan Bui,[5] Rom Leidner,[1,5] Walter J. Urba,[1] Kent Johnson,[6] Clifford Hoyt,[6] Carlo B. Bifulco,[1,7] Juergen Bukur,[8] Claudia Wickenhauser,[3] Barbara Seliger,[8] and Bernard A. Fox[1,9]

[1]Robert W. Franz Cancer Research Center, Earle A. Chiles Research Institute, Portland, Oregon, USA. [2]Department of Cancer Biology, Oregon Health & Science University, Portland, Oregon, USA. [3]Institute of Pathology and [4]Department of Oral and Maxillofacial Plastic Surgery, Martin Luther University Halle-Wittenberg, Halle, Germany. [5]Providence Oral, Head and Neck Cancer Program and Clinic, Providence Cancer Center, Portland, Oregon, USA. [6]PerkinElmer Inc., Hopkinton, Massachusetts, USA. [7]Department of Pathology, Providence Cancer Center, Portland, Oregon, USA. [8]Institute of Medical Immunology, Martin Luther University Halle-Wittenberg, Halle, Germany. [9]Department of Molecular Microbiology and Immunology, Oregon Health & Science University, Portland, Oregon, USA.

Evaluation of T lymphocyte frequency provides prognostic information for patients with oral squamous cell cancer (OSCC). However, the effect of simultaneously evaluating T cell frequency and assessing suppressive elements and defects in antigen-processing machinery (APM) has not been clarified. Simultaneous characterization of CD3$^+$, CD8$^+$, FoxP3$^+$, CD163$^+$, and PD-L1$^+$ cells using multispectral imaging was performed on sections from 119 patients with HPV$^-$ OSCC. Expression of β_2-microglobulin, MHC class I heavy chain, and large multifunctional peptidase 10 was quantified, and all data were correlated with patient outcome. We found that, consistent with previous reports, high numbers of CD8$^+$ T cells at the invasive margin correlated significantly with prolonged overall survival (OS), while the number of FoxP3$^+$ or PD-L1$^+$ cells did not. Compiling the number of FoxP3$^+$ or PD-L1$^+$ cells within 30 μm of CD8$^+$ T cells identified a significant association with a high number of suppressive elements close to CD8$^+$ T cells and reduced OS. Integrating this information into a cumulative suppression index (CSI) increased correlation with OS. Incorporating tumor expression levels of APM components with CSI further improved prognostic power. This multiparametric immune profiling may be useful for stratifying patients with OSCC for clinical trials.

Introduction

Oral squamous cell cancer (OSCC) represents a leading cause of cancer worldwide, with substantial mortality and morbidity. In contrast to other head and neck squamous cell cancer (HNSCC) subtypes, most OSCCs are attributed to smoking and alcohol, and an association with HPV infection is rare (1–4). While treatment with anti-PD-1 was recently shown to improve outcome for some patients with OSCC, a majority of patients progress and die of their disease (5, 6).

Since the risk stratification based on tumor size, lymph node, and distant metastasis (TNM staging), combined with histological grading alone, is not sufficient to predict the prognosis of OSCC patients (7, 8), additional prognostic biomarkers are urgently required. For colorectal cancer (CRC), the infiltration of adaptive immune cells composed of T lymphocytes (CD3) with cytotoxic (CD8) and memory (CD45RO) phenotype located at the invasive margin (IM) and tumor center, and assessed using digital imaging and objective assessment tools, represents a significant independent parameter to predict recurrence and survival (9–11). Similar trends have been reported for other cancer types; however, due to unique characteristics, each histology needs to be evaluated separately (12–14). In contrast, a strong CD3$^+$/CD8$^+$ T cell infiltrate and a high frequency of CD4$^+$CD69$^+$ T cells correlated with increased overall survival (OS) of HNSCC patients (15–17). However, the prognostic effect of the frequency of CD4$^+$CD25$^+$FoxP3$^+$ Tregs remains controversial (18–20). In this context it is noteworthy that most studies analyzing immune surveillance of HNSCC focused either on HPV$^+$ cancers or did not determine the patients' HPV status (21). As HPV$^+$ HNSCCs are frequently associated with

Authorship note: Z. Feng, D. Bethmann, and M. Kappler contributed equally to this work as co–first authors. C. Wickenhauser, B. Seliger, and B.A. Fox contributed equally to this work as co–senior authors.

Conflict of interest: B.A. Fox serves on the PerkinElmer Inc. Health Division Science Advisory Board.

Submitted: February 27, 2017
Accepted: June 6, 2017
Published: July 20, 2017

Reference information:
JCI Insight. 2017;2(14):e93652. https://doi.org/10.1172/jci.insight.93652.

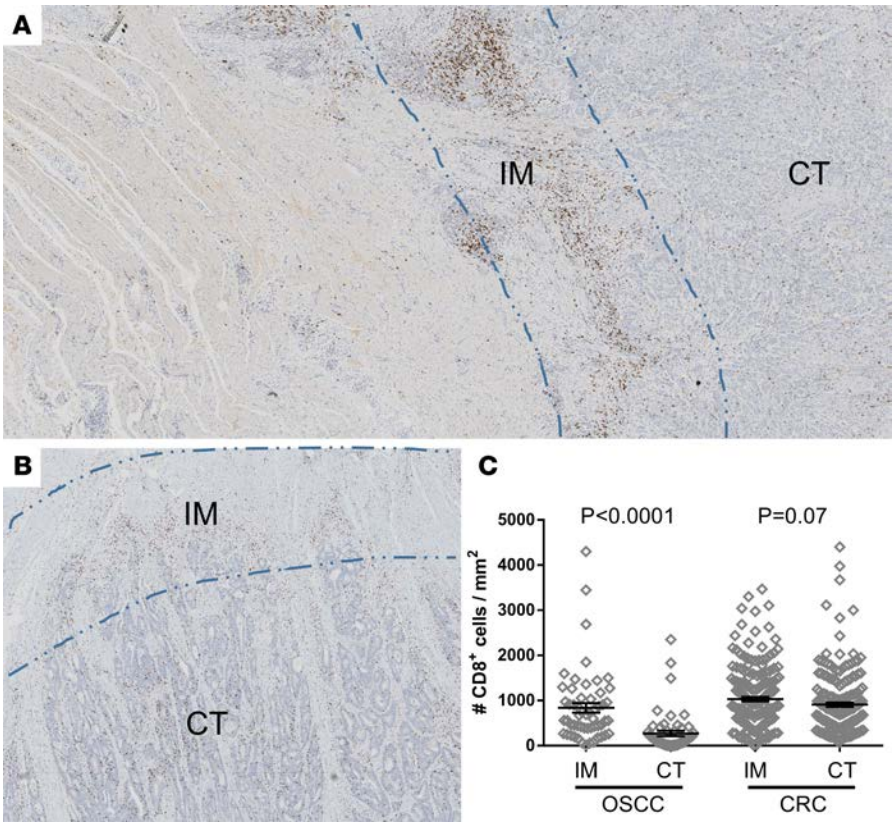


Figure 1. Differences in density and location of immune infiltrate in OSCC, as a typical example of squamous cell carcinoma, compared with colorectal cancer, as a typical example of intestinal adenocarcinoma. (**A**) Representative example with demonstration of topographic position of CD8⁺ infiltrate in OSCC (original magnification, ×40). (**B**) Representative example of CD8⁺ infiltrate in colorectal cancer (CRC) (original magnification, ×40). (**C**) Enumeration of immune cell infiltrate using the Definiens platform. In OSCC, most CD8⁺ cells are located within the stromal side invasive margin (IM), while, in CRC, the majority of CD8⁺ cells are located within the tumor and tumor side IM. Data are represented as dot plots (mean ± SEM). Two-tailed unpaired *t* test was performed to test statistical significance. $n = 55$ for OSCC, $n = 199$ for CRC. CT, core of tumor.

increased T and B cell infiltrates, higher levels of IFN-γ secretion, and increased numbers of FoxP3⁺ T cells, all features of antiviral responses that may translate into enhanced antitumor immune responses (22–26), distinguishing HPV⁺ and HPV⁻ tumors is essential (17, 27).

Immune surveillance is mediated by the composition of the tumor microenvironment (TME); it is affected by a multitude of strategies tumors use to escape immune recognition. These include (a) the lack or downregulation of tumor antigen expression, (b) loss or reduced expression of MHC class I molecules due to impaired expression of components of the antigen-processing machinery (APM), and (c) increased expression of immune-suppressive molecules, like the programmed death-like receptor ligand 1 (PD-L1) and the nonclassical HLA-G and HLA-E antigens (28–31).

So far to our knowledge, a comprehensive analysis of HPV⁻ OSCC, characterizing the composition and location of immune cells within and in close proximity to tumor cells in parallel with an assessment of tumor immune escape mechanisms and association with clinical parameters, has not been performed. In order to get better insights into these processes and their effect on patient survival, which might help in selecting patients with rather adverse prognosis for specific immunotherapies, this study analyzed different components of immune surveillance/escape using multispectral imaging and objective assessment combined with conventional IHC (32, 33).

Results

Density of CD8⁺ T cells at the IM predicts outcome of HPV⁻ OSCC patients. Analysis of HPV⁻ OSCC identified that the IM harbored a more dense immune cell infiltrate than the tumor centers, a difference that was more pronounced than in the published data on CRC (9) (Figure 1). Based on these results, our studies focused on evaluating cells at the IM, which was further divided into tumor and stromal sides of the IM (Figure 2).

A correlation between a high density of CD3⁺CD8⁺ T cells at the IM and improved OS was found (Figure 3, A and B). Through enumeration of CD8⁺ T cells of the IM, we found that the CD8⁺ T cell number on the tumor side had a greater effect on OS than that on the stromal side ($P = 0.01$, Figure 3, A and B), suggesting that, even within the IM, the relative location of CD8⁺ T cells (tumor or stroma) plays a role.

Distance from FoxP3⁺ Tregs to CD8⁺ T cells predicts outcome in HPV⁻ OSCC. While an increased number of CD3⁺ FoxP3⁺ T cells on the stromal side of IM was associated with increased OS, the difference was not

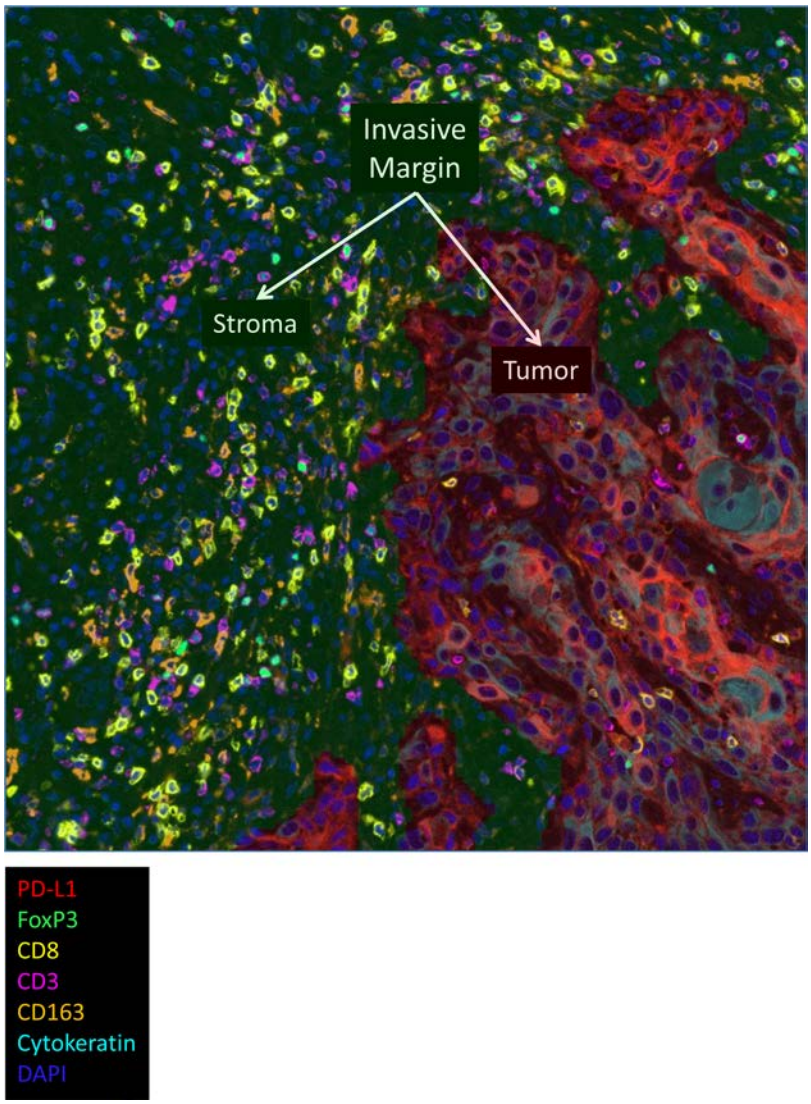


Figure 2. Representative image of immune cell infiltrate in an OSCC tumor. Tissue sections were simultaneously stained for 7 antigens. Images (original magnification, ×20) with a high density of immune cell infiltrate were taken from stromal and tumor side invasive margin. Red overlay, recognized by software as tumor; green overlay, recognized by the software as stroma.

significant (Figure 3, C and D). Similar findings have been reported for CRC, HPV$^+$ OSCC, and gastric cancer (34, 35). Based on a positive correlation between an increased number of Tregs and the CD8$^+$ T cell infiltrate (Figure 4), we posited that Tregs recruited to the TME might not be close enough to the CD8$^+$ T cells to suppress their effector function. To investigate this hypothesis, the local density of FoxP3$^+$ T cells around each CD8$^+$ T cell was determined for the tumor and stromal side of the IM and normalized for CD8$^+$ T cells. Preliminary analysis of 34 tumor cases revealed that an increased number of Tregs within 30 μm of CD8$^+$ cells ($FoxP3_{30\mu m}CD8n$) was associated with worse outcome (Figures 5 and 6). Extrapolating this formula to the entire cohort of 119 patients identified a highly significant correlation, with significantly worse OS for patients with higher numbers of FoxP3$^+$ T cells within 30 μm of CD8$^+$ T cells; this was true on the stromal and tumor side of the IM (Figure 7, A and B). We next evaluated whether the FoxP3/CD8 ratio would provide a similar prognostic power to that seen above. For both the tumor and stromal sides of the IM, the FoxP3/CD8 ratio, while trending in the same direction as the $FoxP3_{30\mu m}CD8n$ evaluation, failed to provide a prognostic signature that was statistically significant (Figure 7, C and D). These data suggest that Tregs more proximal to CD8$^+$ T cells are more effective at suppressing anticancer function.

Distance from PD-L1$^+$ cells to CD8$^+$ T cells and PD-L1/CD8 ratio predict outcome in HPV$^-$ OSCC. Since enumeration of PD-L1$^+$ cells had no correlation with outcome (Figure 3, E and F), we evaluated the effect of

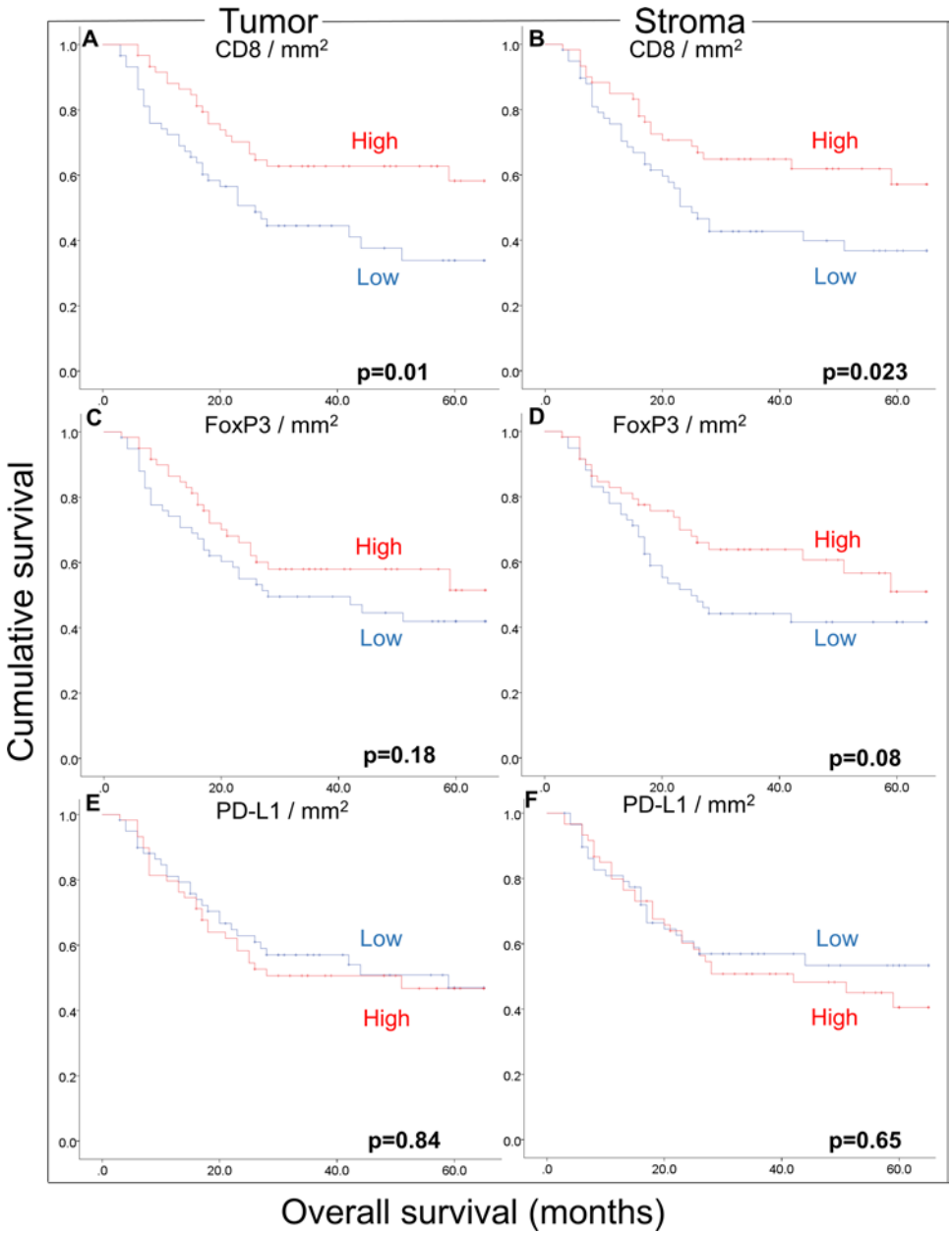


Figure 3. Effect of immune infiltrate density at the invasive margin on overall survival. Higher densities of CD8⁺, but not FoxP3⁺, T cells and PD-L1⁺ tumor cells at the invasive margin (IM) predict favorable OS, while this effect is more profound on the stromal side of the IM. Densities of CD8, FoxP3, and PD-L1 on both the tumor and stromal sides of the IM were enumerated using PerkinElmer inForm software. A median cutoff was used to separate high and low infiltrate. Log-rank statistics were performed to determine significance. *n* = 119.

having more PD-L1⁺ cells within 30 μm of CD8⁺ T cells (PD-L1$_{30\mu m}$CD8n). Patients with a high number of PD-L1⁺ cells within 30 μm of CD8⁺ T cells, normalized to CD8 T cell numbers, had a significantly worse outcome (Figure 8, A and B), with the effect being greatest for cells on the stromal side of the IM ($P < 0.0005$). We also found that the ratio of PD-L1/CD8⁺ cells for both the stromal and tumor side of the IM provided a strong biomarker for OS (Figure 8, C and D).

Combining assessment of suppressive elements further separates patient populations. Since suppression mediated by FoxP3⁺ and PD-L1⁺ cells would be expected to be additive, we created a suppression index (SI) based on the variables enumerated above: specifically, the number of FoxP3⁺ cells and the number of PD-L1⁺ cells within 30 μm of a CD8⁺ T cell, normalized to CD8⁺ T cell numbers. Patients who were in the top 50% for both categories were in the high SI category and had the worst OS. Patients who were in the top 50%

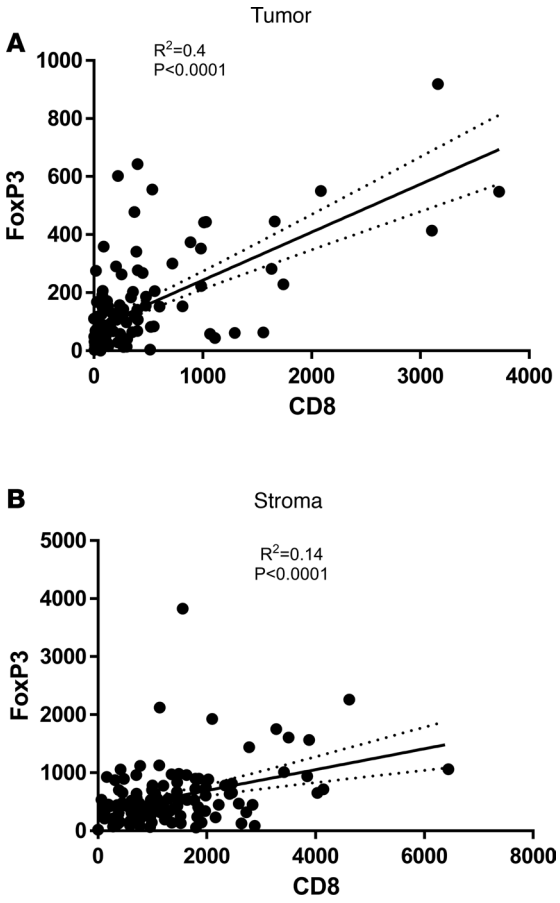


Figure 4. Independent analysis and correlation of CD8⁺/FoxP3⁺ immune cell infiltrates at the tumor and stromal side of the invasive margins. (**A**) Tumor side and (**B**) stromal side. Data are represented in a scattered plot with the best fit (solid line) and 95% confidence interval (dotted line) shown. Statistical test for *P* values was linear regression. *n* = 124 for both tumor and stroma.

for one category were intermediate. Those in the lower 50% for both FoxP3 and PD-L1 had the lowest SI and the highest OS. Evaluating the SI for both the tumor and stromal side of the IM provided a highly significant prognostic biomarker for OS (Figure 9).

The SI is a strong prognostic marker, independent of tumor size and UICC stage. To compare the well-known International Union Against Cancer (UICC) tumor-staging prognostic system with the SI, the OSCC cohort was separated into two groups based on OS (Figure 10). Patients with UICC stage III disease were grouped with those with UICC stage I and II disease based on their coinciding approximately 70% 5-year OS. The SI was highly predictive for OS independent of OSCC UICC stage (I–III), particularly on the stromal side of the IM, as patients with the lowest SI here achieved almost 90% 5-year OS compared with less than 40% for patients with the highest SI (Figure 11, A and B). The median cut point for the FoxP330um CD8n cells for the tumor and stromal side (Figure 11, C and D) did not provide a significant separation in OS, but the stromal side tended to show a better separation of the curves. The same analysis of the PD-L130umCD8n cells was not significant for the tumor side, but evaluation of the stromal side provided a significant ($P = 0.007$) prognostic biomarker for OS (Figure 11, E and F) In patients with stage IV disease, the SI had the potential to discriminate patients with different disease course, in particular by evaluating the tumor side of the IM rather than the stromal site (Figure 12, A and B). Here the median cut point for the FoxP330um CD8n cells for the tumor side, but not the stromal side, provided a significant ($P = 0.003$) separation in OS (Figure 12, C and D). In the case of PD-L130umCD8n cells the median cut point for both the tumor and stromal sides of the tumor provided a significant ($P = 0.019$ and $P = 0.05$, respectively) prognostic marker of OS, but the tumor side, as seen for FoxP3, tended to give better separation of the curves (Figure 12, E and F).

APM defects associated with worse outcome. As defects in antigen presentation represent immune escape strategies of tumors that can define disease outcome, these were assessed using MHC class I β_2-microglobulin (β_2m) and heavy chain (HC) as well as the large multifunctional peptidase 10 (LMP10). Using chromogenic IHC, patients with high (international rating score [IRS] 4–12) versus low (IRS 0–3) cytoplasmic expression levels of β_2m showed a tendency toward a worse OS (relative risk [RR] of death 1.64, $P = 0.08$), independent of T- and N-stage as well as grading, though this effect did not reach statistical significance (Figure 13A). This effect was predominantly accounted for in patients with UICC stage I–II tumors (RR 2.77, $P = 0.07$, Figure 13B), rather than in those with UICC stage III–IV tumors (RR 1.23, $P = 0.54$). In contrast, a high membranous β_2m expression level was not a predictive biomarker in this study. Staining results for cytoplasmic expression of HC10 mAb were in concordance with cytoplasmic β_2m data showing a strong yet insignificant trend toward worse OS (RR 1.6, $P = 0.08$) in patients with high versus low cytoplasmic class I HC expression levels. No difference could be seen as dividing UICC stage I–II versus UICC stage III–IV tumors or membranous β_2m expression levels. Regarding LMP10, patients with high versus low cytoplasmic expression showed a slight yet insignificant trend toward worse OS (RR 1.44, $P = 0.28$). No differences were detected when dividing patients based on their UICC stage or in nuclear LMP10 level expression. Cumulative results regarding the cytoplasmic expression of the three APM components are shown in Figure 14A.

Cumulative SI provides greater prognostic power for HPV⁻ OSCC. By combining the SI generated from the stromal and tumor side of the IM, a cumulative suppressive index (CSI) was generated (Figure 14B). This CSI scoring system combines the evaluation of FoxP3⁺ and PD-L1⁺ within 30 μm of CD8⁺ T cells at both the stromal and tumor side of the IM. Each time a patient was in the top 50% for their cohort, they received 1 point. If they were in the top 50% for all 4 assessments, they could receive a total of 4 points (Figure 14B). Applying the CSI to all patients (Figure 14C), or to stage I–III (Figure 14D) or stage IV patients (Figure 14E), identified patients with a

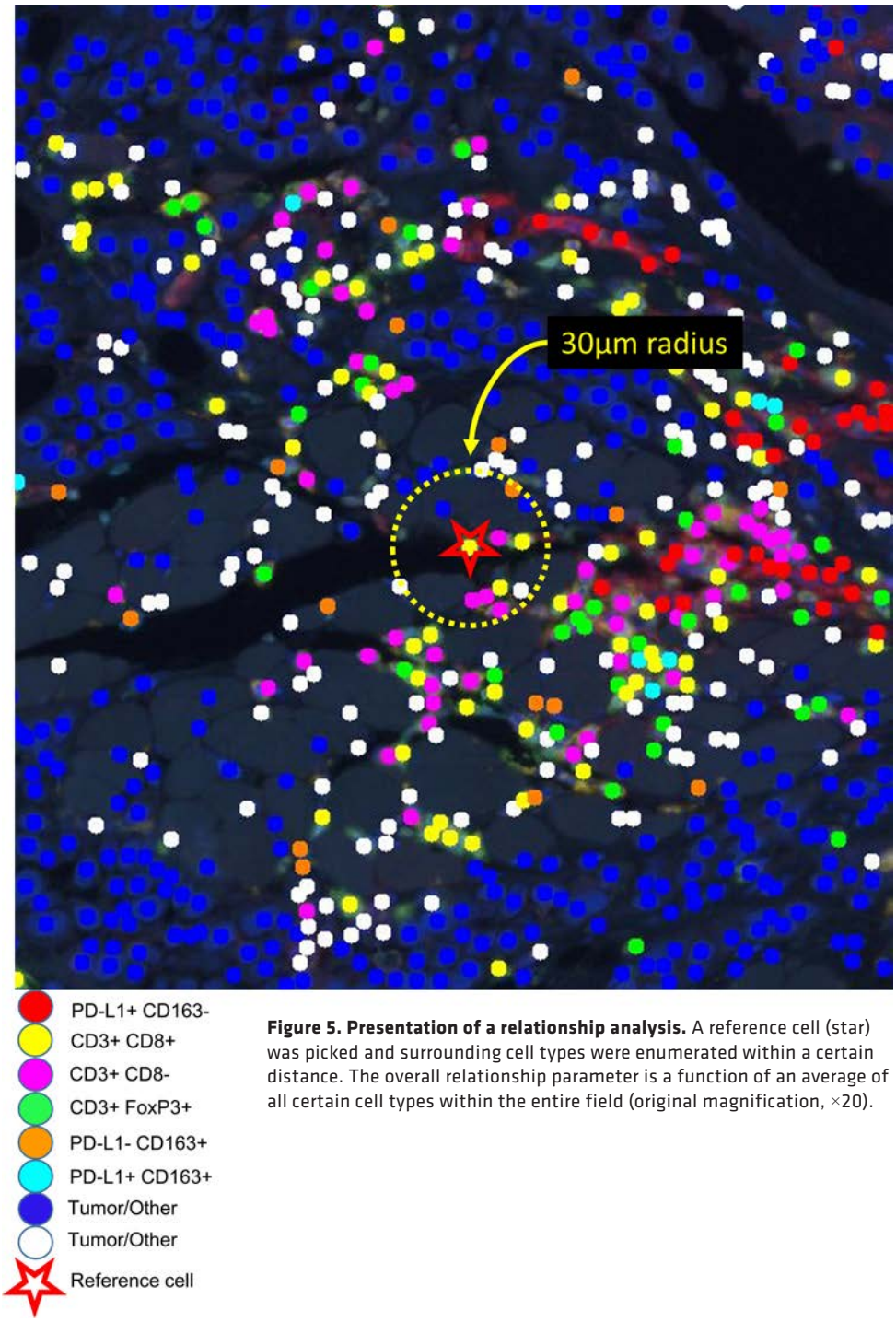


Figure 5. Presentation of a relationship analysis. A reference cell (star) was picked and surrounding cell types were enumerated within a certain distance. The overall relationship parameter is a function of an average of all certain cell types within the entire field (original magnification, ×20).

significant probability to do worse had the highest CSI. Even with patients with stage IV disease, patients with a CSI score of 0 had a 60% 5-year survival compared with those with a score of 4, who rapidly succumbed to their disease (Figure 14E). Thus, even for patients with late-stage HPV$^-$ OSCC, the CSI is still meaningful for separation of OSCC patients with rather good clinical outcome from those with poor clinical outcome.

Evaluating the effect of MHC class I β_2m and HC as well as LMP10 expression levels, we also identified that the effect of defects in these pathways could be additive, with patients with defects in all 3 pathways having the worst outcome (Figure 14A). Since these defects were independent of the FoxP3- and PD-L1–mediated suppression, we combined both the CSI and the APM defects. In doing so, we created an 8-point scoring system, ranging from 0 to 7 (Figure 14F). Each point, or category, is based on a median

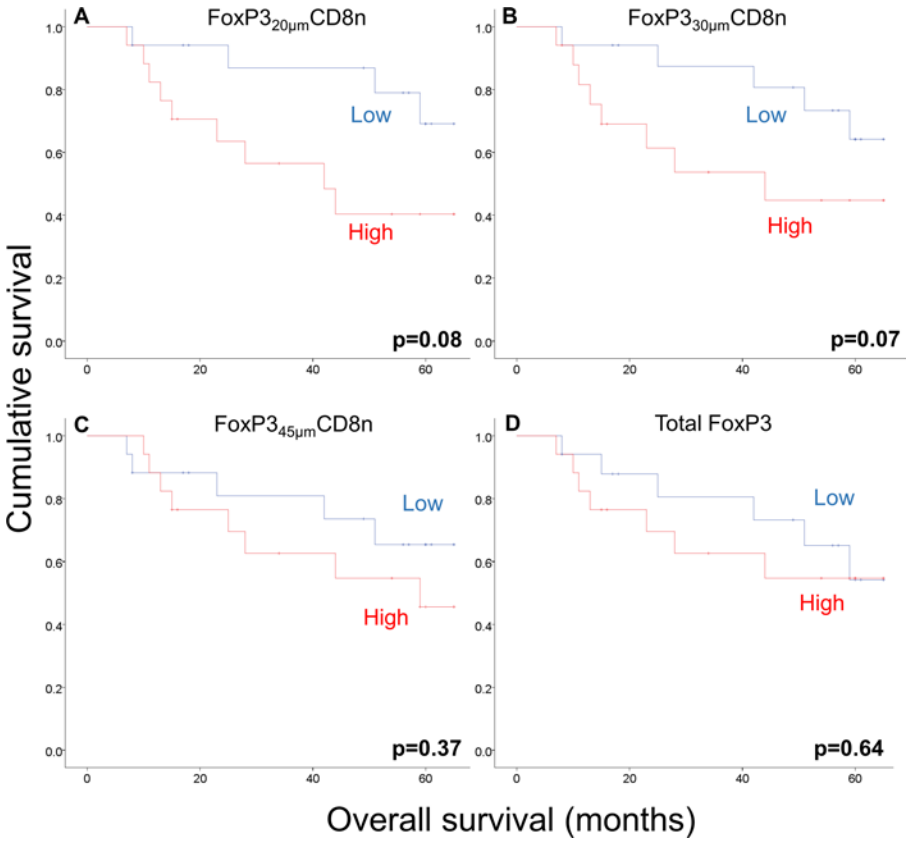


Figure 6. Optimization of the cutoff of the distance of FoxP3$^+$ cells within specified distance of CD8$^+$ T cells, normalized for CD8$^+$ T cell number. Cumulative survival for a test cohort of 34 patients characterized as being above (high) or below (low) the median for FoxP3$_{20\mu m}$CD8n (**A**), FoxP3$_{30\mu m}$CD8n (**B**), FoxP3$_{45\mu m}$CD8n (**C**), and total FoxP3 (**D**). The number of FoxP3$^+$ T cells within 30 μm of a CD8$^+$ T cell, normalized to number of CD8$^+$ T cells (FoxP3$_{30\mu m}$CD8n) (**B**), provides the best statistical cutoff point and was therefore used for the analysis of the entire cohort of patients. Numbers of FoxP3$^+$ T cells and distance were determined using PerkinElmer inForm and R script and were normalized to the number of CD8$^+$ T cells (FoxP3$_{30\mu m}$CD8n). A median cutoff was used to separate high and low infiltrate. Kaplan-Meier survival plots were made, and statistics were generated using log-rank test. n = 34.

cutoff. A score of 7 would imply that all categories (PD-L1 and FoxP3 suppression in tumor and stroma as well as APM defects that include the cytoplasmic portions of β_2m, HC10, and LMP10) were above the median cutoff. In contrast, patients with a score of 0 would be in the lowest group for all inhibitory mechanisms specified. This CSI plus cytoplasmic APM index provided a striking and highly significant separation of patients; for patients given a score of 0, 100% survived 5 years, and for those given a score of 7, all the patients had died within 30 months of follow-up time.

Discussion

This immune profiling study objectively assessed not only the frequency and composition of the immune cell infiltrate, but also the cell-to-cell topography and thereby the probability of cell-to-cell interactions, with additional correlation to clinical and prognostic parameters. Multispectral imaging performed on HPV$^-$ OSCC enabled us to objectively assess 6 markers and quantify the number of cells expressing that marker and their cartographic coordinates on one 4-μm section of FFPE tissue (33).

Based on the density, composition, and localization of immune cell infiltrates, in particular of CD8$^+$ T cells, the immunoscore was developed, which had independent prognostic relevance in CRC, in addition to other cancer types (36–38). In regards to HNSCC, various immune subsets have been correlated with clinical outcome (39, 40), but the majority of these reports either focused exclusively on HPV$^+$ HNSCC or did not distinguish patient populations based on the HPV status. However, high-throughput analyses revealed that HPV$^+$ and HPV$^-$ HNSCCs are two distinct clinical entities, which have specific molecular features and an altered immune phenotype characterized by CD8$^+$ T cell infiltration (40).

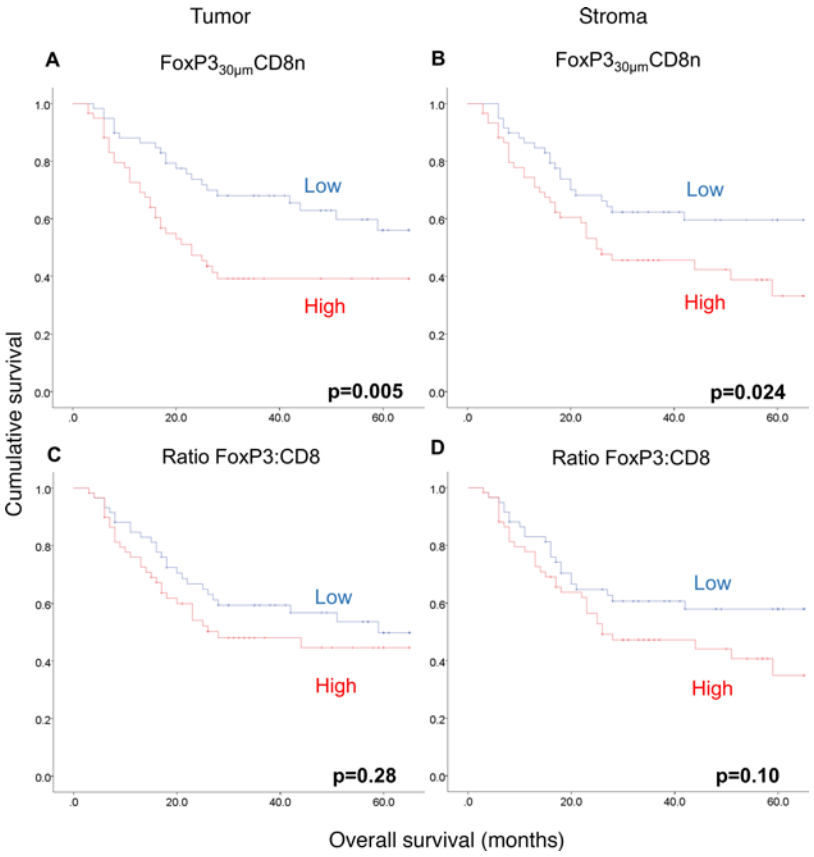


Figure 7. Effect of topographic distance of FoxP3$^+$ T cells from CD8$^+$ T cells on prognosis. A high number of FoxP3$^+$ cells within 30 μm of CD8$^+$ T cells, normalized to CD8$^+$ T cell numbers (FoxP3$_{30\mu m}$CD8n), on the tumor (**A**) and the stromal (**B**) side of the invasive margin present a significant prognostic marker for worse OS, while the ratio of FoxP3/CD8 T cells failed to provide a significant prognostic signature (**C** and **D**). Absolute numbers of T cells as well as distance relationship were determined using PerkinElmer inForm and R script and were normalized to the number of CD8$^+$ T cells. A median cutoff was used to separate high and low distance relationships. Kaplan-Meier survival plots were made, and statistics were generated using log-rank test. *n* = 119.

To date, our study, consisting of 119 patients from two centers, represents one of the largest HPV$^-$ OSCC studies. Consistent with other reports, our results indicated a favorable association between high CD8$^+$ T cell density and OSCC patient survival (41). By focusing exclusively on CD8$^+$ T cells on the tumor side of the IM, long-term survivors were identified independent from tumor stage, suggesting a prognostic value of the immune cell repertoire in the TME. In contrast to our data, an inverse correlation between tumor PD-L1 expression and outcome of HNSCC patients has recently been shown in a Chinese cohort (42), which might be at least partially explained by the lack of distinction of the HPV status and/or a distinct pathogenesis among ethnic groups. This might be of great impact, as high PD-L1 expression levels can be mediated by external stimuli, including cytokines secreted from immune cells, or intrinsic constitutive expression due to gene amplification (43), utilization of an ectopic promoter by translocation (44), disruption of the 3′ untranslated region of PD-L1 (45), or aberrant signaling pathways (46).

Based on our previous data in melanoma (32), we investigated the ratios as well as the spatial relationship between CD8$^+$ T cells and immune suppressors. Adapted from an optimal separation of a test cohort of 34 patients (Figure 6), FoxP3 and PD-L1 expression was analyzed within a 3-lymphocyte-wide distance (30 μm) around CD8 T cells; the numbers of FoxP3$^+$ and PD-L1$^+$ cells were normalized to the total number of CD8 T cells, and this number was equal to the SI. By normalizing the number of FoxP3 and PD-L1 cells to CD8$^+$ T cells in the region of interest, this SI takes into consideration both the active suppressive mechanisms, FoxP3$^+$ and PD-L1$^+$ cells as well as an overall "suppressed" or absent anticancer immune response, characterized by a low number of CD8 T cells. Using this approach, OSCC patients with a low SI survived much longer compared with those with a high SI, while the OS for those with an intermediate SI fell right in the middle. Upon separating the patients by tumor stage, the stromal SI was more important in stage I–III patient, while the tumor SI appeared to be more important in stage IV patients. These results lead to the hypothesis that, in earlier tumor stages, without apparent organ metastases, the most important function of stromal immune infiltrate involves the control of tumor spreading, while in late-stage tumors with apparent organ metastases, tumor-infiltrating immune cells represent a favorable signature. Next, we combined the SI of the stromal and the tumor side of the IM to create the CSI and found that patients with the highest CSI had reduced survival. To further strengthen

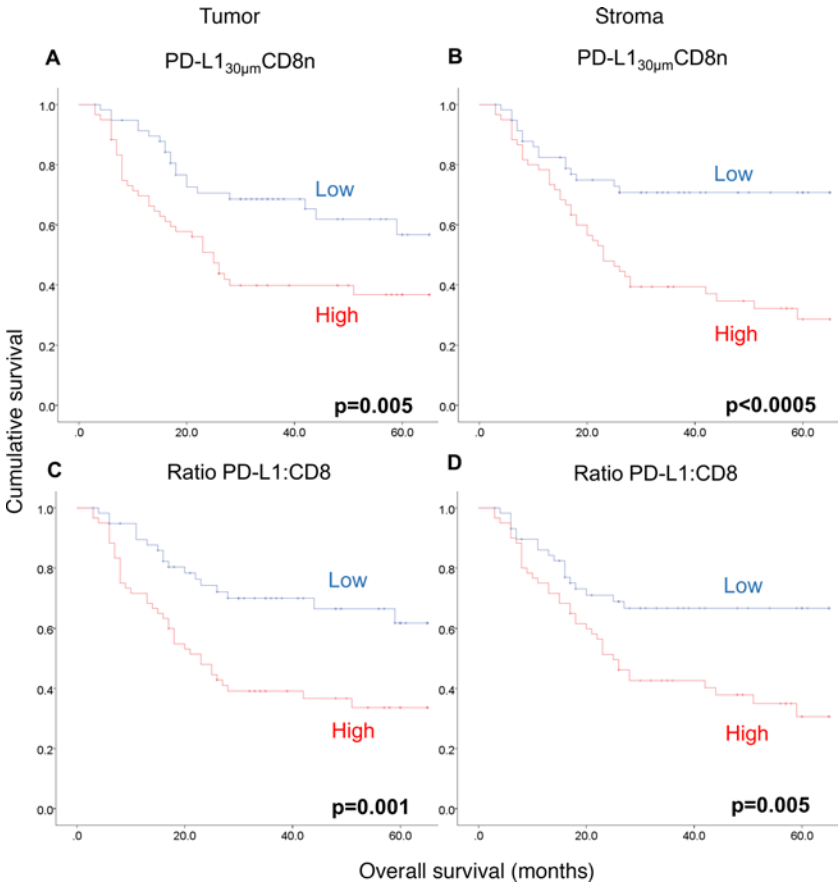


Figure 8. Effect of topographic distance of PD-L1$^+$ T cells from CD8$^+$ T cells on prognosis. A high number of PD-L1$^+$ within 30 μm of CD8$^+$ T cells (PD-L1$_{30\mu m}$CD8n) (**A** and **B**) as well as the ratio of PD-L1/CD8 T cells (**C** and **D**) on the tumor and the stromal side of the invasive margin present a significant prognostic marker for worse OS. Absolute numbers of T cells as well as distance relationship were determined using PerkinElmer inForm and R script and were normalized to the number of CD8$^+$ T cells. A median cutoff was used to separate high and low distance relationships. Kaplan-Meier survival plots were made, and statistics were generated using log-rank test. *n* = 119.

our scoring system, the expression of APM components was determined. The cytoplasmic expression of APM components inversely correlated with OS of OSCC patients (Figure 14A). Thus, higher cytoplasmic expression of HC and β_2m might indicate a defect in the export of MHC class I molecules to the cell surface, a mechanism already described in virus-infected cells, leading to reduced T cell–mediated killing (47). So far, altered MHC class I APM component expression in HNSCC and other cancers has been documented by others but has not been correlated to the immune cell infiltrate of the tumor specimen (48–50). The underlying molecular mechanisms of the disturbed APM component expression have not been analyzed in detail, but deregulation, rather than structural abnormalities, appears to be main cause (51). By combining APM parameters with CSI, patients with a 100% 5-year survival could be identified and distinguished from those who rapidly progressed, with none surviving at 30 months. Our study, while small in size and in need of validation, not only confirms the importance of CD8$^+$ T cells in prognosis, but also highlights the complexity of the TME, suggesting that the assessment of multiple parameters is necessary in order to better identify those patients in need of more aggressive treatment strategies. Future research should include a validation cohort and should evaluate whether to weigh suppressive elements or APM by some other factor than the median score and evaluate whether that may further improve outcome prediction of the presented index. For that matter, the predictive value of other APM components (e.g., TAP1/2, calreticulin/calnexin, ERp57, ERAP1/2) should also be tested. Additionally, our process of normalizing the FoxP3 and PD-L1 relationships within 30 μm of a CD8 T cell to the number of CD8 T cells includes a reduced number of CD8 T cells as a component of the suppressive index. This reduced CD8 T cell number may represent the result of active suppression, but, in many patients with "cold" tumors, it may be indicative of the absence of an immune response and not actual

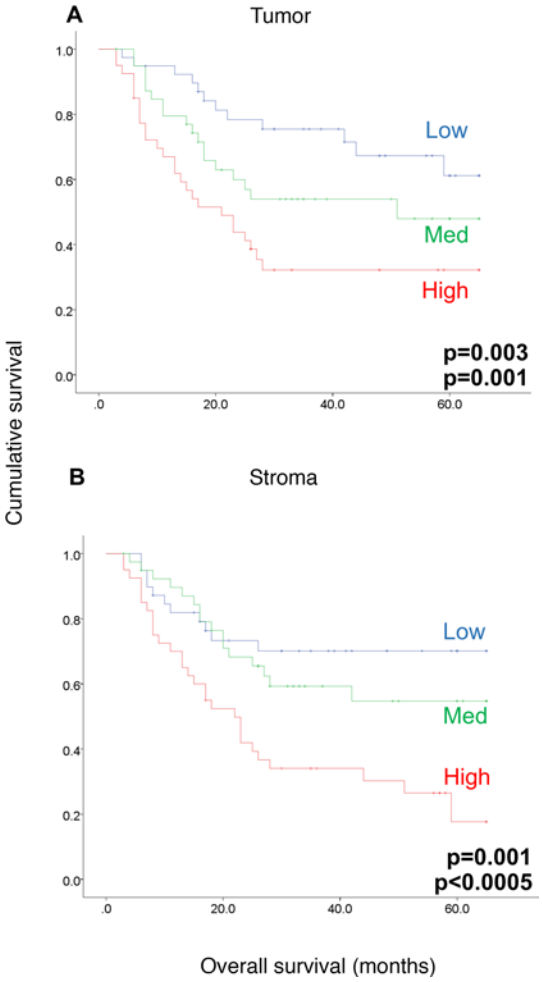


Figure 9. Effect of a suppression index on prognosis. Use of a suppression index (SI) incorporating both the number of FoxP3$^+$ cells and the number of PD-L1$^+$ cells within 30 μm of a CD8$^+$ T cell, normalized to CD8$^+$ T cell number, on both the tumor (**A**) and the stromal (**B**) side of the invasive margin separates patients into 3 distinct prognostic groups, providing a highly significant biomarker. Here, the expressions based on median cutoff of $FoxP3_{30\mu m}CD8n$ and $PD\text{-}L1_{30\mu m}CD8n$ were added together and ranked from high (score of 2) to low (score of 0). Patients who were in the top 50% for both categories were in the high SI category and had the worst OS. Patients who were in the top 50% for one category were intermediate, and those in the lower 50% for both $FoxP3_{30\mu m}CD8n$ and $PD\text{-}L1_{30\mu m}CD8n$ had the lowest SI and the highest OS. Log-rank statistics were performed to determine significance. The top *P* value refers to all comparisons, the bottom *P* value refers to the difference between the lowest and highest score. $n = 119$.

suppression. This could have important ramifications for clinical trial design by identifying patients who need an adoptive immunotherapy or a cancer vaccine as a component of their combination immunotherapy. Furthermore, the separation we identified supports evaluation of the CSI in additional histologies. A limitation of these studies is the substantial user input for staining and evaluation of multispectral images; for example, these include manual staining protocols and the selection of regions of interest, spectral libraries, and exposure times in inForm, which are prone to interobserver variability. In our opinion, what is needed now is to move multiplex immunohistochemical staining to an automated CLIA platform, make improvements to image acquisition technology to optimize signal strength for each slide,

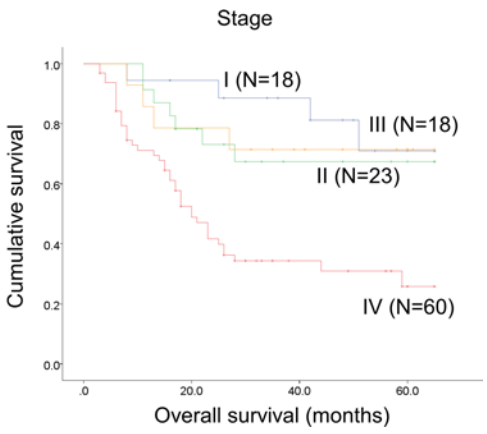


Figure 10. Stage distribution and basic patient characteristics. Kaplan-Meier survival plot of the cohort based on UICC stage.

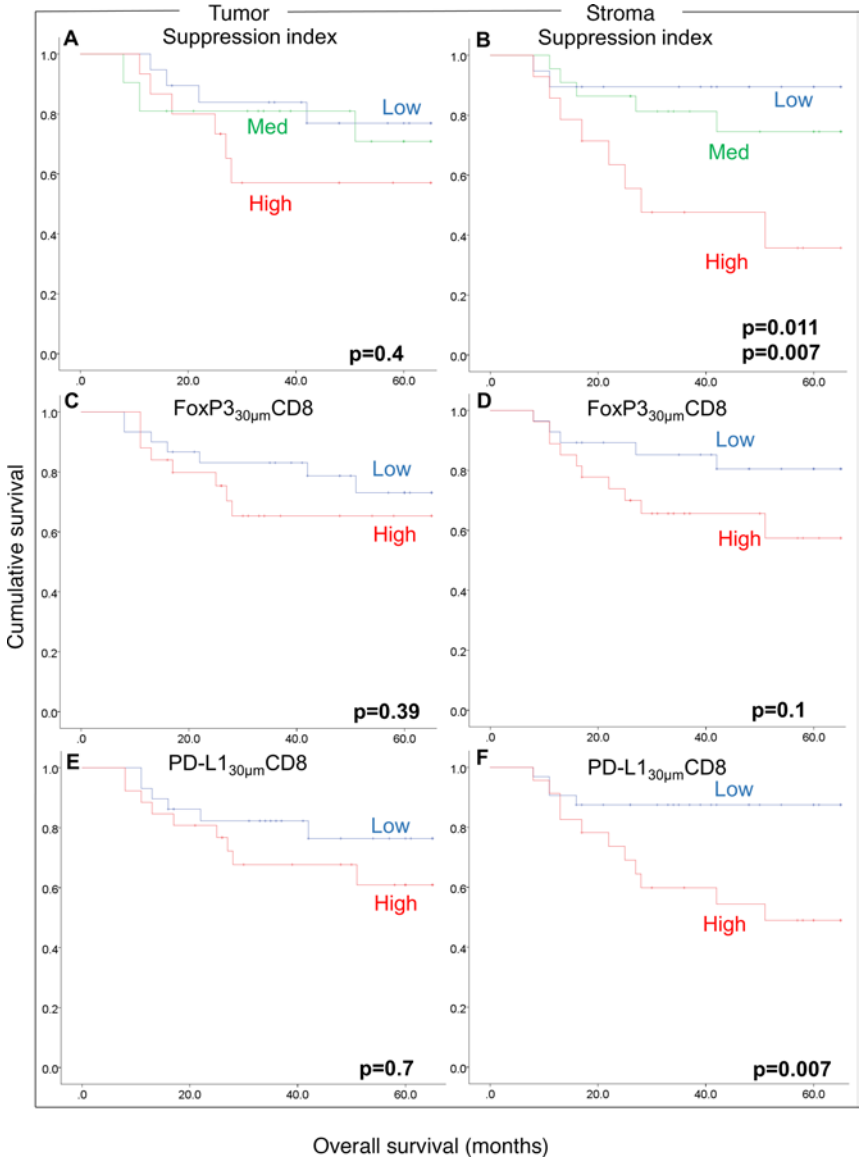


Figure 11. Effect of the suppression index and distance relationships on OS in stage I–III OSCC patients. (**A** and **B**) Using a suppression index (SI) incorporating both FoxP3$_{30\mu m}$CD8n and PD-L1$_{30\mu m}$CD8n presents a significant prognostic marker for OS on the stromal side (**B**) but not on the tumor side of the invasive margin (IM) (**A**). (**C–F**) In stage I–III OSCC patients, only a high number of PD-L1$_{30\mu m}$CD8n cells on the stromal side of the IM (**F**) presents a significant biomarker, marking an unfavorable OS. For **A** and **B**, ranks were assigned as presented in Figure 9. For **C–F**, a median cutoff was used to separate high and low distance relationships. Kaplan-Meier survival plots were made, and statistics were generated using log-rank test. *n* = 59.

modify software so that it can automatically identify regions of interest, and accelerate the time required to complete the analyses. Moving forward, we are working with collaborators to test improved image analysis algorithms and are evaluating automated multiplex staining methods. Successful development and application of these tools should lead to accelerated analysis times and validated panels that could be used in "real-time" clinical decision making.

Overall, these data, while preliminary and in need of validation, are consistent with a large body of work and signify the importance of T cell responses in HPV$^-$ OSCC. They provide a rationale for the utilization of multiplex imaging in characterizing the possible escape mechanisms operational in a given patient. It is our vision that this type of assessment, which may include additional markers and possibly other methodologies (52), will ultimately allow for the precise tailoring of combination immunotherapy agents and aid in identifying patients that may require treatment intensification.

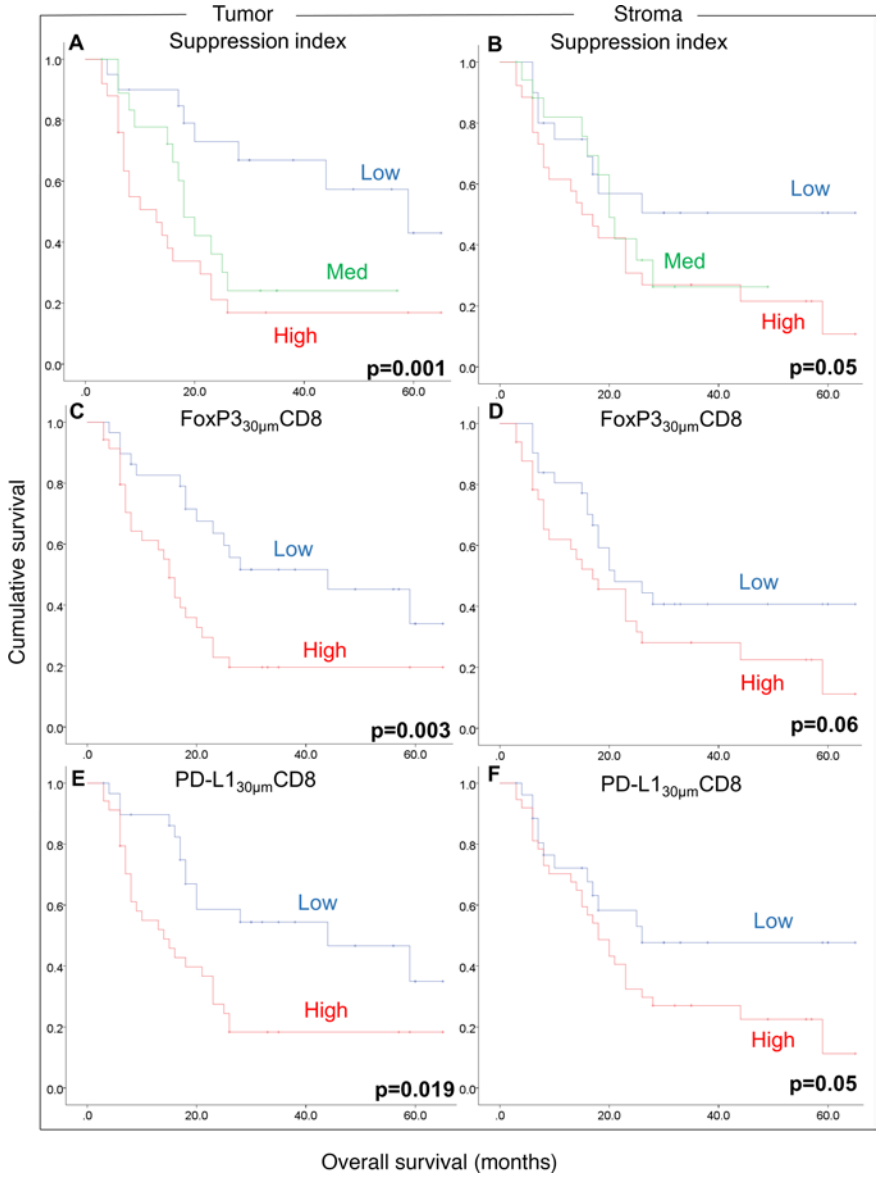


Figure 12. Effect of the suppression index and distance relationships on OS in stage IV OSCC patients. (**A** and **B**) Using a suppression index (SI) incorporating both the FoxP3$_{30\mu m}$CD8n and the PD-L1$_{30\mu m}$CD8n provides a significant prognostic marker for OS on both the tumor (**A**) and the stromal side of the invasive margin (IM) (**B**), with a more profound effect on the tumor side (**A**). (**C–F**) A high number of FoxP3$_{30\mu m}$CD8n (**C**) and PD-L1$_{30\mu m}$CD8n (**E**) cells on the tumor side of the IM provides a significant biomarker, identifying an unfavorable OS. For **A** and **B**, ranks were assigned as presented in Figure 9. For **C–F**, a median cutoff was used to separate high and low distance relationships. Kaplan-Meier survival plots were made, and statistics were generated using log-rank test. *n* = 60.

Methods

Study population and selection criteria. The study included 152 OSCC primary tumors from Halle, Germany, and 12 OSCC primary tumors from Portland, Oregon, USA. Forty-five patients were dropped from the study due to HPV positivity or lack of IM in the tumor slides, resulting in 119 patients being available for study. UICC stage distribution as well as basic patient characteristics are summarized in Figure 10 and Tables 1 and 2.

Bright-field IHC and analysis. For bright-field IHC, the mAbs NAMB (β_2m; SP09-36), HC10 (HLA class I HC; HSP09-35), and TO-7 (LMP10; SP08-225) were used (30). Tissue samples were deparaffinized with xylol and transferred via alcohol into aqua dest (Elix 5 Filter System, Merck-Millipore). Antigen decloaking was performed by steaming the slides with a preheated T-EDTA buffer (ZUC029-500, 1:10 dilution, Zytomed Systems) at pH 9.0 and 98°C for 20 minutes in an oven (Braun, type 3216). After cool-

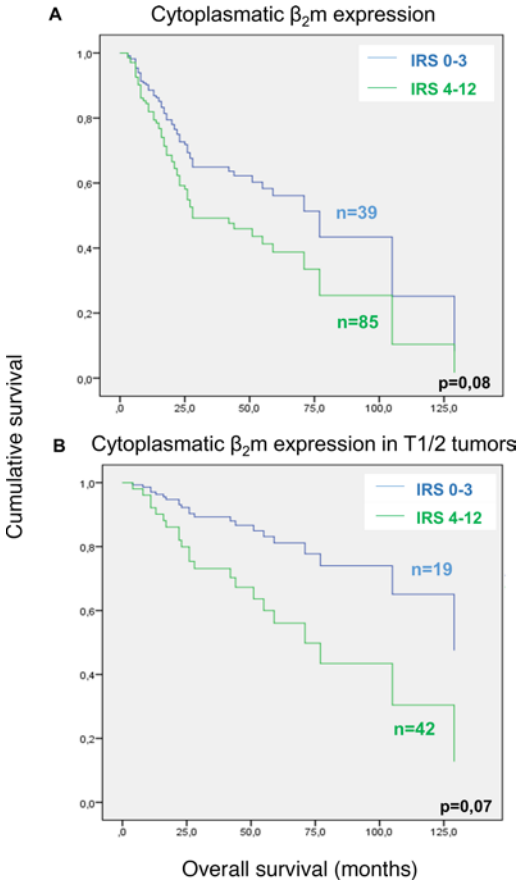


Figure 13. Effect of cytoplasmic expression of β_2m on OS. (**A**) Kaplan-Meier curve highlighting the strong yet insignificant tendency toward a prognostic effect of high levels of cytoplasmic expressed β_2m (IRS 4–12 vs. 0–3), leading to a 1.64-fold increase (P = 0.08) in the relative risk (RR) of death, independent of T- and N-stage and grading. (**B**) This effect was predominantly accounted for by patients with T1–2 stage tumors (RR 2.77, P = 0.07), rather than in T3–4 stage tumors (RR 1.23, P = 0.54, data not shown).

ing down for 20 minutes and rinsing with aqua dest, slides were blocked for 7–10 minutes with 3% H_2O_2. Following another rinsing step and application of washing buffer (ZUC202-2500, 1:20 solution, Zytochem Plus HRP Kit/Plus Polymer System, Zytomed), the antibodies β_2m (1:50 dilution), HC10 (1:2,500 dilution), and LMP10 (1:200 dilution) were added dropwise on the tissue area and incubated for 30 minutes at room temperature. Antibody removal was performed by vacuum followed by a washing step. Then, slides were incubated with a biotinylated secondary antibody (Broad Spectrum, Zytochem Plus HRP Kit, Zytomed) for 15 minutes at room temperature and rinsed with washing buffer, followed by 15 minutes of incubation with HRP (Zytochem Plus HRP, Zytomed). The epitopes were visualized with DAB (10 minutes, DAB Substrate Kit, Zytomed). After further rinsing steps (aqua dest), the slides were counterstained with hemalaun (Dr. K. Hollborn & Sons) for 30 seconds, transferred into xylol, and covered (Eukitt, ORSAtec) for bright-field analysis.

Staining results were semiquantitatively evaluated utilizing the IRS, as described by Remmele et al. (53). In short, staining intensity (0, negative; 1, low; 2, moderate; 3, strong positive) and the percentage of stained cells (0, negative; 1, <10%; 2, 10%–50%; 3, 51%–80%; 4, >80%) were evaluated, and the IRS score was then calculated as the product of the two, ranging from 0–12. Tissue samples were independently categorized by two pathologists (CW and DB). Ten percent of all cases plus all cases presenting any technical challenges were coreviewed by both pathologists to harmonize and ensure reproducibility of the APM scoring. All the remaining cases were scored by one pathologist (DB).

Multiplex IHC and analysis. Multispectral imaging was performed as previously described in detail in the supplemental section of Feng et al. (32) with minor changes, using mAbs directed against PD-L1 (E1L3N, Cell Signaling), CD8 (M239, Spring Bioscience), FoxP3 (236A/E7, Abcam), CD3 (2GV6, Ventana, prediluted, incubation for 45 minutes), CD163 (MRQ26, Ventana), and cytokeratin (AE1/AE3, DAKO, 1:100 dilution, incubation for 45 minutes) as well as DAPI (Invitrogen). TSA-Cy5 (PerkinElmer Inc.), TSA-Cy3 (PerkinElmer Inc.), TSA-FITC (PerkinElmer Inc.), TSA-Alexa594 (Life Technologies), TSA-Biotin-Alexa514 (PerkinElmer Inc., Life Technologies), and TSA-Coumarin (PerkinElmer Inc.) were applied to each antibody. Slides were imaged using the PerkinElmer Vectra platform. A "hotspot" analysis was performed. Three ×20 fields from the IM were manually selected based on the highest lymphocytic infiltrate. Tumor (cytokeratin$^+$) and stromal (cytokeratin$^-$) areas within hotspots were identified using inForm software (example in Figure 2), and cell number and cartographic coordinates (distance from each cell and location within tumor or stroma) for each cell were obtained (example Figure 5). Images were analyzed in small batches using PerkinElmer inForm and R script for cell phenotype enumeration and relationship analysis. Cells that were positive for both CD3 and CD8 were classified as CD8$^+$. Cells that were CD3$^+$ and had nuclear staining for FoxP3 were considered FoxP3$^+$. Except for CD3$^+$PD-L1$^+$ double-positive cells, any cell that expressed PD-L1 was considered a PD-L1$^+$ cell. This includes both tumor cells and macrophages. Evaluation of FoxP3$^+$ and PD-L1$^+$ within 30 μm of a CD8 T cell, normalized to the number of CD8 T cells, was performed by first obtaining the number of FoxP3$^+$ or PD-L1$^+$ cells within 30 μm of a CD8 T cell and then normalizing that to the number of CD8 T cells according to the following formula: number of FoxP3 within 30 μm of a CD8 T cell/total CD8s = $FoxP3_{30\mu m}CD8n$. The median number of $FoxP3_{30\mu m}CD8n$ was 1.93×10^{-3} for the tumor and 1.28×10^{-3} A for the stromal side of the invasive margin. A similar formula was applied for characterizing PD-L1: number of PD-L1$^+$ macrophages and tumor cells within 30 μm of a CD8 T cell/total CD8s = $PD\text{-}L1_{30\mu m}CD8n$. The median number of $PD\text{-}L1_{30\mu m}CD8n$ was 1.32×10^{-3} for the tumor and 1.25×10^{-3} A for the stromal side of the invasive margin.

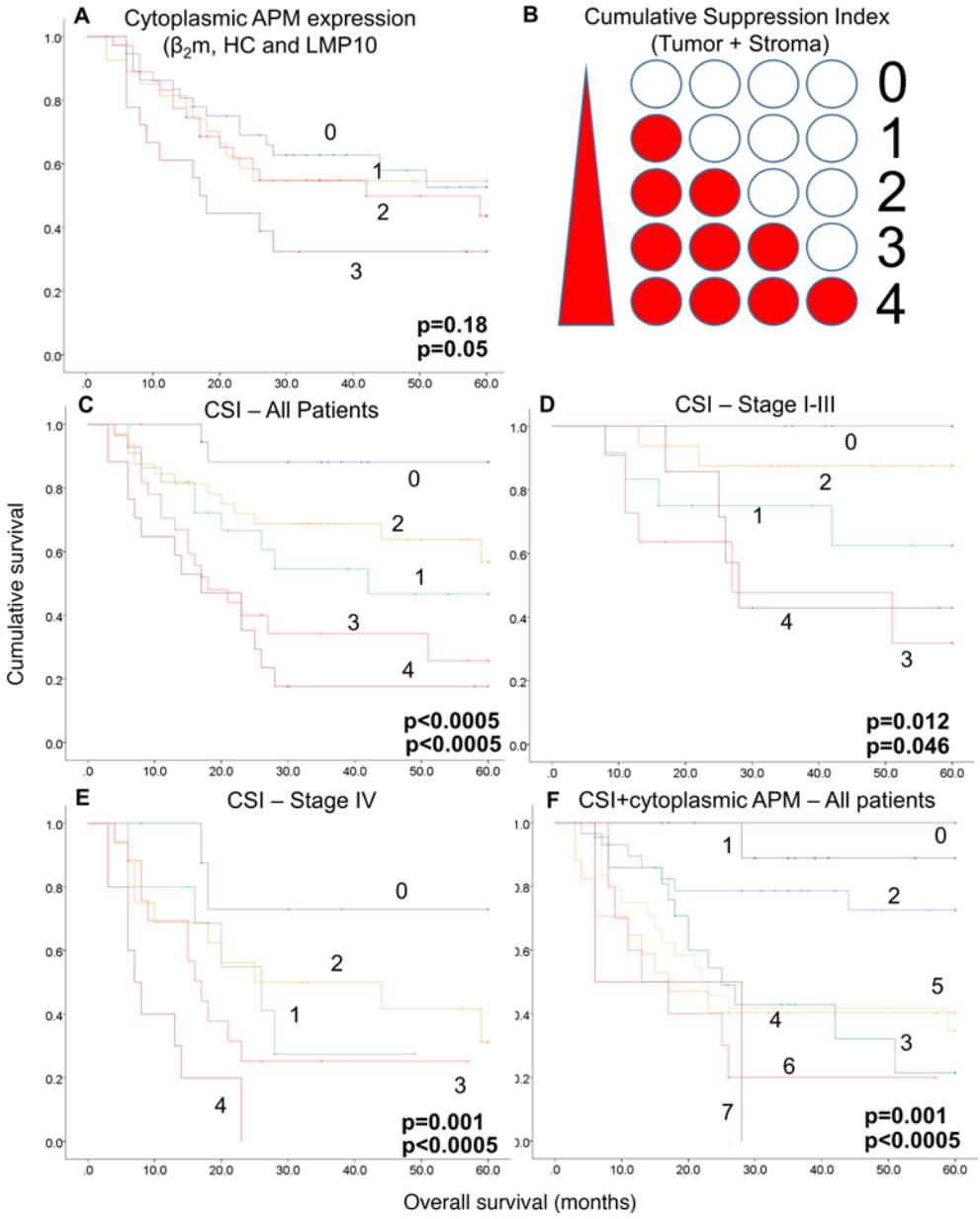


Figure 14. The cumulative suppression index is a highly indicative prognostic marker superior to the prognostic index of the single markers. (**A**) Kaplan-Meier curve showing the influence of the combined cytoplasmatic expression levels of β_2m, HC, and LMP10 on OS. Patients were separated as above or below the median for each marker. A score of 0 represents below-median cutoff expression, and a score of 3 represents high expression for all three APM components. (**B**) Combining suppression indices (SI) from tumor and stroma to obtain cumulative suppression index (CSI). Each column represents $FoxP3_{30\mu m}CD8n$ and $PD\text{-}L1_{30\mu m}CD8n$ in tumor and stroma, with red indicating above-median cutoff, marking increased suppression. (**C**) Analysis of the entire cohort demonstrates the highly significant stepwise reduction of OS based on an increasing CSI, with 0 representing the lowest and 4 representing the most suppression relative to $CD8^+$ T cells. (**D**) Kaplan-Meier curve for the CSI for patients with stage I–III disease. (**E**) Kaplan-Meier curve for the CSI for patients with stage IV disease. (**F**) Analysis of CSI in combination with the 3 APM components, demonstrating a highly significant stepwise reduction of OS based on an increasing score. A score of 0 represents low suppression and low cytoplasmatic APM expression (below-median cutoff); a score of 7 represents high (above-median) cutoff for all 7 categories. (**A** and **C**–**F**) Log-rank statistics were performed to determine significance. The top *P* value refers to all comparisons, the bottom *P* value refers to the difference between the lowest and highest score. *n* = 119 (**A**, **C**, and **F**); 59 (**D**); **E** = 60 (**E**).

Statistics. Statistical analyses for bright-field IHC were performed using SPSS 20.0 software (SPSS Inc.). To evaluate survival probabilities in patients with low group sizes, two groups (low vs. high protein expression levels) were selected for each marker based on an even distribution of patients' scores in these groups. IHC results were then correlated with clinical data using univariable and multivariable Cox

Table 1. Cohort age, stage, grade, and follow-up data

	Age(yr)	Follow-up (mo)	Stage	Grade
No.	119	119	119	119
Median	58	26	3	2
Minimum	22	3	1	1
Maximum	83	60	4	3

regression analysis. In multivariable Cox regression, T- and N-stage and grading were included as confounding factors. Survival probability was visualized using Kaplan-Meier graphs. A *P* value of less than 0.05 was considered as significant result. For Figure 1, 2-tailed unpaired *t* tests were performed using PRISM, and a *P* value of less than 0.05 was considered significant.

For multiplex IHC, medians for all presented immune markers are summarized in Table 3. For multiplex data, Kaplan-Meier survival curves were established using SPSS statistical software v23. For Figures 3, 6–12, and 14, a median cutoff was used, log-rank and Breslow tests were performed, and a *P* value from the most appropriate test was reported. A *P* value of less than 0.05 was considered significant. For SI studies, a binary value for each category was assigned based on a median cutoff, the sum of all values was used to generate the SI score. Analyses were appropriately corrected for multiple comparisons when comparing two or more groups. Multivariate Cox regression incorporating stage and grade was performed where applicable. A *P* value of less than 0.05 was considered significant. For Figure 4, linear regression was performed using PRISM, and 95% confidence interval is shown. R^2 value is shown, and a *P* value of less than 0.05 was considered significant.

Study approval. The study was carried out in compliance with the Helsinki Declaration. The study was approved by the ethics committee of the Medical Faculty of Martin Luther University Halle-Wittenberg and the institutional review board of the Providence Portland Medical Center (12-075A).

Author contributions

BS, CW, CBB, RBB, and BAF participated in the conception or design of the work. ZF, DB, MK, CBM, AE, RBB, AC, and TB contributed to data acquisition. ZF, DB, MK, BS, CW, CBM, AE, RBB, AC, TB, RL, WJU, KJ, HC, CBB, JB, and BAF participated in data analysis and interpretation. ZF, DB, BS, CW, CBB, and BAF participated in drafting the manuscript. All authors contributed to the critical revision and had final approval of the version to be published.

Acknowledgments

This work was supported by the Murdoch Trust (to BAF), the Oregon Clinical and Translational Research Institute (TL1TR000129 to ZF) through the National Center for Advancing Translational Sciences at the NIH, the Providence Medical Foundation, the Oral Maxofacial Surgery Foundation (to RBB, CBB, and BAF), Bob and Elsie Franz, the Chiles Foundation, Wes and Nancy Lematta, the Harder Family, Lynn and Jack Loacker (to BAF), and the Deutsche Krebshilfe project (to BS).DB would like to thank the histology lab at the Institute of Pathology at the Halle University Clinic and, in particular, Jana Beer for comprehensive help with this study.

Table 2. Cohort sex, treatment, and survival percentages

Male (%)	62.0
Received radiation (%)	40.0
Received chemotherapy (%)	100.0
HPV^- cases (%)	51.8
Survival at last follow-up (%)	75.9

Table 3. Medians for all presented immune markers

	Tumor	Stroma
CD4	43 cells/mm^2	784 cells/mm^2
CD8	116 cells/mm^2	1127 cells/mm^2
FoxP3	74 cells/mm^2	437 cells/mm^2
Total PD-L1	867 cells/mm^2	432 cells/mm^2

Address correspondence to: Barbara Seliger, Institute of Medical Immunology, Martin Luther University Halle-Wittenberg, Magdeburger Str. 2, 06112 Halle (Saale), Germany. Phone: 49.345.557.4054; Email: barbara.seliger@uk-halle.de. Or to: Bernard A. Fox, Robert W. Franz Cancer Research Center, Earle A. Chiles Research Institute, 4805 NE Glisan Street, 2N56, Portland, Oregon, USA. Phone: 01.503.215.6614; Email: bernard.fox@providence.org.

1. Abreu LP, Kruger E, Tennant M. Oral cancer in Western Australia, 1982-2006: a retrospective epidemiological study. *J Oral Pathol Med*. 2010;39(5):376–381.
2. Listl S, et al. Survival of patients with oral cavity cancer in Germany. *PLoS One*. 2013;8(1):e53415.
3. Rogers SN, et al. Survival following primary surgery for oral cancer. *Oral Oncol*. 2009;45(3):201–211.
4. Zini A, Czerninski R, Sgan-Cohen HD. Oral cancer over four decades: epidemiology, trends, histology, and survival by anatomical sites. *J Oral Pathol Med*. 2010;39(4):299–305.
5. Pulte D, Brenner H. Changes in survival in head and neck cancers in the late 20th and early 21st century: a period analysis. *Oncologist*. 2010;15(9):994–1001.
6. Chow LQM et al. Antitumor activity of pembrolizumab in biomarker-unselected patients with recurrent and/or metastatic head and neck squamous cell carcinoma: results from the phase Ib KEYNOTE-012 expansion cohort. *J Clin Oncol*. 2016;34(32):3838–3845.
7. Lothaire P, et al. Molecular markers of head and neck squamous cell carcinoma: promising signs in need of prospective evaluation. *Head Neck*. 2006;28(3):256–269.
8. Piazzolla D, et al. Lineage-restricted function of the pluripotency factor NANOG in stratified epithelia. *Nat Commun*. 2014;5:4226.
9. Galon J, et al. Type, density, and location of immune cells within human colorectal tumors predict clinical outcome. *Science*. 2006;313(5795):1960–1964.
10. Broussard EK, Disis ML. TNM staging in colorectal cancer: T is for T cell and M is for memory. *J Clin Oncol*. 2011;29(6):601–603.
11. Mlecnik B, et al. Integrative analyses of colorectal cancer show immunoscore is a stronger predictor of patient survival than microsatellite instability. *Immunity*. 2016;44(3):698–711.
12. Fridman WH, Pagès F, Sautès-Fridman C, Galon J. The immune contexture in human tumours: impact on clinical outcome. *Nat Rev Cancer*. 2012;12(4):298–306.
13. Bethmann D, Feng Z, Fox BA. Immunoprofiling as a predictor of patient's response to cancer therapy-promises and challenges. *Curr Opin Immunol*. 2017;45:60–72.
14. Halama N, et al. Localization and density of immune cells in the invasive margin of human colorectal cancer liver metastases are prognostic for response to chemotherapy. *Cancer Res*. 2011;71(17):5670–5677.
15. Balermpas P, et al. Tumour-infiltrating lymphocytes predict response to definitive chemoradiotherapy in head and neck cancer. *Br J Cancer*. 2014;110(2):501–509.
16. Russell S, et al. Immune cell infiltration patterns and survival in head and neck squamous cell carcinoma. *Head Neck Oncol*. 2013;5(3):24.
17. Pretscher D, Distel LV, Grabenbauer GG, Wittlinger M, Buettner M, Niedobitek G. Distribution of immune cells in head and neck cancer: CD8+ T-cells and CD20+ B-cells in metastatic lymph nodes are associated with favourable outcome in patients with oro- and hypopharyngeal carcinoma. *BMC Cancer*. 2009;9:292.
18. Lim KP, et al. CD4+CD25hiCD127low regulatory T cells are increased in oral squamous cell carcinoma patients. *PLoS One*. 2014;9(8):e103975.
19. Schwarz S, Butz M, Morsczeck C, Reichert TE, Driemel O. Increased number of CD25 FoxP3 regulatory T cells in oral squamous cell carcinomas detected by chromogenic immunohistochemical double staining. *J Oral Pathol Med*. 2008;37(8):485–489.
20. Strauss L, Bergmann C, Szczepanski M, Gooding W, Johnson JT, Whiteside TL. A unique subset of CD4+CD25highFoxp3+ T cells secreting interleukin-10 and transforming growth factor-beta1 mediates suppression in the tumor microenvironment. *Clin Cancer Res*. 2007;13(15 Pt 1):4345–4354.
21. Schlecht NF, et al. Gene expression profiles in HPV-infected head and neck cancer. *J Pathol*. 2007;213(3):283–293.
22. Stransky N, et al. The mutational landscape of head and neck squamous cell carcinoma. *Science*. 2011;333(6046):1157–1160.
23. Koch WM, Lango M, Sewell D, Zahurak M, Sidransky D. Head and neck cancer in nonsmokers: a distinct clinical and molecular entity. *Laryngoscope*. 1999;109(10):1544–1551.
24. Wilczynski SP, Lin BT, Xie Y, Paz IB. Detection of human papillomavirus DNA and oncoprotein overexpression are associated with distinct morphological patterns of tonsillar squamous cell carcinoma. *Am J Pathol*. 1998;152(1):145–156.
25. Wansom D, et al. Correlation of cellular immunity with human papillomavirus 16 status and outcome in patients with

advanced oropharyngeal cancer. *Arch Otolaryngol Head Neck Surg*. 2010;136(12):1267–1273.
26. King EV, Ottensmeier CH, Thomas GJ. The immune response in HPV(+) oropharyngeal cancer. *Oncoimmunology*. 2014;3(1):e27254.
27. Partlová S, et al. Distinct patterns of intratumoral immune cell infiltrates in patients with HPV-associated compared to non-virally induced head and neck squamous cell carcinoma. *Oncoimmunology*. 2015;4(1):e965570.
28. Bukur J, Jasinski S, Seliger B. The role of classical and non-classical HLA class I antigens in human tumors. *Semin Cancer Biol*. 2012;22(4):350–358.
29. Seliger B. Novel insights into the molecular mechanisms of HLA class I abnormalities. *Cancer Immunol Immunother*. 2012;61(2):249–254.
30. Seliger B, Quandt D. The expression, function, and clinical relevance of B7 family members in cancer. *Cancer Immunol Immunother*. 2012;61(8):1327–1341.
31. Whiteside TL. Tumor-induced death of immune cells: its mechanisms and consequences. *Semin Cancer Biol*. 2002;12(1):43–50.
32. Feng Z, et al. Multispectral imaging of formalin-fixed tissue predicts ability to generate tumor-infiltrating lymphocytes from melanoma. *J Immunother Cancer*. 2015;3:47.
33. Stack EC, Wang C, Roman KA, Hoyt CC. Multiplexed immunohistochemistry, imaging, and quantitation: a review, with an assessment of Tyramide signal amplification, multispectral imaging and multiplex analysis. *Methods*. 2014;70(1):46–58.
34. Shang B, Liu Y, Jiang SJ, Liu Y. Prognostic value of tumor-infiltrating FoxP3+ regulatory T cells in cancers: a systematic review and meta-analysis. *Sci Rep*. 2015;5:15179.
35. Ma GF, et al. High FoxP3 expression in tumour cells predicts better survival in gastric cancer and its role in tumour microenvironment. *Br J Cancer*. 2014;110(6):1552–1560.
36. Maby P, et al. Correlation between density of Cd8+ T-cell infiltrate in microsatellite unstable colorectal cancers and frameshift mutations: a rationale for personalized immunotherapy. *Cancer Res*. 2015;75(17):3446–3455.
37. Galon J, et al. Towards the introduction of the 'Immunoscore' in the classification of malignant tumours. *J Pathol*. 2014;232(2):199–209.
38. Bindea G, et al. Spatiotemporal dynamics of intratumoral immune cells reveal the immune landscape in human cancer. *Immunity*. 2013;39(4):782–795.
39. Green VL, Michno A, Stafford ND, Greenman J. Increased prevalence of tumour infiltrating immune cells in oropharyngeal tumours in comparison to other subsites: relationship to peripheral immunity. *Cancer Immunol Immunother*. 2013;62(5):863–873.
40. Rittà M, et al. Cell cycle and viral and immunologic profiles of head and neck squamous cell carcinoma as predictable variables of tumor progression. *Head Neck*. 2009;31(3):318–327.
41. de Winde CM, Zuidscherwoude M, Vasaturo A, van der Schaaf A, Figdor CG, van Spriel AB. Multispectral imaging reveals the tissue distribution of tetraspanins in human lymphoid organs. *Histochem Cell Biol*. 2015;144(2):133–146.
42. Lin YM, et al. High PD-L1 expression correlates with metastasis and poor prognosis in oral squamous cell carcinoma. *PLoS One*. 2015;10(11):e0142656.
43. Saito R, Abe H, Kunita A, Yamashita H, Seto Y, Fukayama M. Overexpression and gene amplification of PD-L1 in cancer cells and PD-L1(+) immune cells in Epstein-Barr virus-associated gastric cancer: the prognostic implications. *Mod Pathol*. 2017;30(3):427–439.
44. Georgiou K, et al. Genetic basis of PD-L1 overexpression in diffuse large B-cell lymphomas. *Blood*. 2016;127(24):3026–3034.
45. Kataoka K, et al. Aberrant PD-L1 expression through 3'-UTR disruption in multiple cancers. *Nature*. 2016;534(7607):402–406.
46. Lee Y, et al. CD44+ cells in head and neck squamous cell carcinoma suppress t-cell-mediated immunity by selective constitutive and inducible expression of PD-L1. *Clin Cancer Res*. 2016;22(14):3571–3581.
47. Tudor CS, et al. c-Myc and EBV-LMP1: two opposing regulators of the HLA class I antigen presentation machinery in epithelial cells. *Br J Cancer*. 2012;106(12):1980–1988.
48. Meissner M, et al. Defects in the human leukocyte antigen class I antigen processing machinery in head and neck squamous cell carcinoma: association with clinical outcome. *Clin Cancer Res*. 2005;11(7):2552–2560.
49. Bandoh N, et al. HLA class I antigen and transporter associated with antigen processing downregulation in metastatic lesions of head and neck squamous cell carcinoma as a marker of poor prognosis. *Oncol Rep*. 2010;23(4):933–939.
50. Leone P, Shin EC, Perosa F, Vacca A, Dammacco F, Racanelli V. MHC class I antigen processing and presenting machinery: organization, function, and defects in tumor cells. *J Natl Cancer Inst*. 2013;105(16):1172–1187.
51. Feenstra M, et al. Mutation in the beta 2m gene is not a frequent event in head and neck squamous cell carcinomas. *Hum Immunol*. 1999;60(8):697–706.
52. Yuan J, et al. Novel technologies and emerging biomarkers for personalized cancer immunotherapy. *J Immunother Cancer*. 2016;4:3.
53. Remmele W, Stegner HE. [Recommendation for uniform definition of an immunoreactive score (IRS) for immunohistochemical estrogen receptor detection (ER-ICA) in breast cancer tissue]. *Pathologe*. 1987;8(3):138–140.